TURBULENT IMPINGING JET INTO A POROUS BED WITH VARYING SOLID-TO-FLUID THERMAL CONDUCTIVITY RATIO

Felipe Tannús Dórea, dorea@ita.br
Marcelo J. S. de Lemos, delemos@ita.br
Departamento de Energia - IEME
Instituto Tecnológico de Aeronáutica - ITA
12228-900 - São José dos Campos - SP, Brazil

Abstract. *This work shows numerical results for a turbulent impinging jet against a flat plane covered with a layer of porous material considering the thermal non-equilibrium. Macroscopic time-averaged equations for mass and momentum are obtained based on a concept called double decomposition, which considers spatial deviations and temporal fluctuations of flow properties using two macroscopic equations of energy: One for the fluid and another for the solid are applied. Turbulence is handled with a macroscopic k–e model, which uses the same set of equations for both the fluid layer and the porous matrix. The numerical technique employed is the control volume method in conjunction with a boundary-fitted coordinate system. One unique computational grid is used to compute the entire heterogeneous medium. The SIMPLE algorithm is applied to relax the system of algebraic equations.*

Keywords*: Ratio* k_s/k_f *,Thermal Non-Equilibrium, Porous Media, Turbulence*

1. INTRODUCTION

Pioneering studies considering two-dimensional impinging jets with low Reynolds number, also onto uncovered flat walls, are presented in Gardon and akfirat (1966), who experimentally obtained local and averaged heat transfer coefficients. Sparrow and Wong (1975) made use of the well-known heat and mass transfer analogy and took experimental data on local mass transfer for a two-dimensional impinging jet. Results were then converted to heat transfer using the mentioned technique. Chen et al. (2000) experimentally and numerically analyzed mass and heat transfer induced by a two-dimensional laminar jet. Chiriac ad Ortega (2002) performed numerical simulations in steady and transitory regime for a two-dimensional jet impinging against a plate with constant temperature.

Recently many studies have been conducted of flow and heat transfer in porous media, including flows parallel to a layer of porous material Kuznetsov et al. (2002) through permeable structures Santos and de Lemos (2006) and porous inserts Assato et al. (2005). Studies of impinging jets into a porous media can be used in order to replace finned surfaces for porous layers, as shown in Figure 1 below:

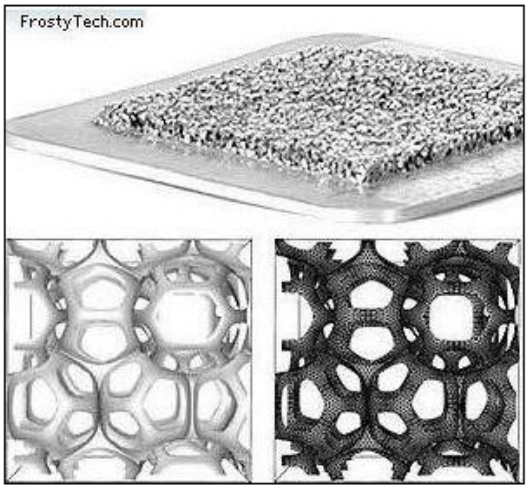

Figure 1- Porous layer used as an alternative to finned surfaces (Extracted from FrostyTech.com in 18/05/2010)

As mentioned, for the specific case here investigated, *i.e*., an impinging jet over a covered plate, there are not too many results in the open literature, being one example the work of Prakash et al. (2001 *a*,*b*) who obtained a flow visualization of turbulent jets impinging against a porous medium. Also, Fu and Huang (1997) evaluated the thermal performance of different porous layers under a impinging jet and Jeng and Tzeng (2005) studied the hydrodynamic and thermal performance of a jet impinging on a metallic foam.

The objective of the present contribution is to extend the investigation of Dórea and de Lemos (2010a) which made use of a laminar formulation of heat and mass transfer in porous media to analyze the effect of solid-to-fluid thermal conductivity ratio applying now a Turbulent formulation.

2. PROBLEM DESCRIPTION

The geometries and nomenclature of the problem are presented in detailed form in Figure 2. A turbulent jet with uniform velocity v_o and constant temperature T_o enters through a gap into a channel with height H and length $2L$. Fluid impinges normally against the bottom plate yielding a two-dimensional confined impinging jet configuration. The width of the inlet nozzle is B and the bottom plate temperature, T_1, is maintained constant and 38.5K above the temperature of the incoming jet, T_o. In a different configuration, the bottom surface is covered with a porous layer of height h (Figure 2*b*). In both cases, the flow is assumed to be two-dimensional, turbulent, incompressible and steady. Also, the porous medium is taken to be homogeneous, rigid and inert. Fluid properties are constant and gravity effects are neglected.

The boundary conditions for the problem are: a) constant velocity and temperature profiles of the entering jet, b) no slip condition on the walls, c) symmetry condition in $x = 0$, d) fully developed flow at channel exit ($x = L$). At the bottom plate ($y = H$), constant temperature condition is assumed whereas along the upper wall, for $B/2 < x \le L$, null heat flux condition prevails.

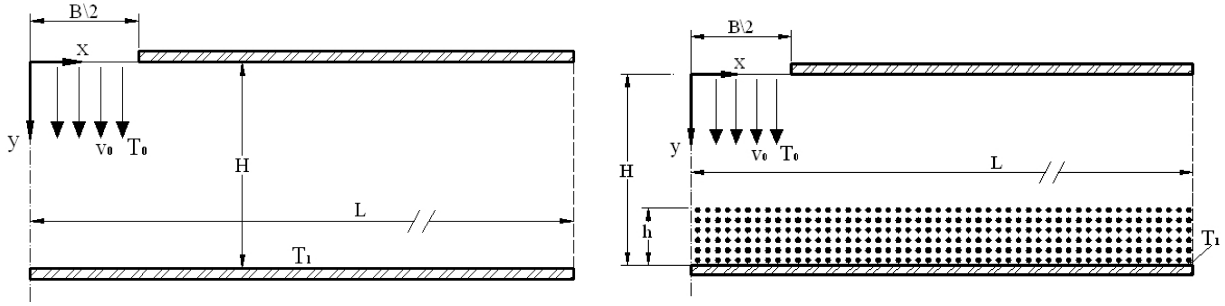

(a) (b)

Figure 2– Cases Investigated (a) Clean Medium (b) Porous Medium

3. MATHEMATICAL MODELING

The most of theoretical development is readily available in the open literature, the governing equations will be just presented and details about their derivations can be obtained in the mentioned papers. Essentially, local instantaneous equations are volume-averaged using appropriate mathematical tools. Accordingly for turbulent flow, the equations read:

Macroscopic continuity equation

The macroscopic equation of continuity for an incompressible fluid flowing through a porous medium is given by:

$$\nabla \cdot \overline{\mathbf{u}}_D = 0 \tag{1}$$

where, $\overline{\mathbf{u}}_D = \phi \langle \overline{\mathbf{u}} \rangle^i$ and $\langle \overline{\mathbf{u}} \rangle^i$ identifies the intrinsic (liquid) average of the time-averaged velocity vector $\overline{\mathbf{u}}$

Macroscopic momentum equation:

The macroscopic momentum equation (Navier-Stokes) for an incompressible fluid with constant properties (ρ and μ constants) flowing through a porous medium, can be written as:

$$\rho\left[\frac{\partial \overline{\mathbf{u}}_D}{\partial t} + \nabla \cdot \left(\frac{\overline{\mathbf{u}}_D \overline{\mathbf{u}}_D}{\phi}\right)\right] = -\nabla(\phi \langle \overline{p} \rangle^i) + \mu \nabla^2 \overline{\mathbf{u}}_D - \nabla \cdot (\rho \phi \langle \overline{\mathbf{u}'\mathbf{u}'} \rangle^i) - \left[\frac{\mu \phi}{K} \overline{\mathbf{u}}_D + \frac{c_F \phi \rho |\overline{\mathbf{u}}_D| \, \overline{\mathbf{u}}_D}{\sqrt{K}}\right] \tag{2}$$

where the last two terms in equation (2) represent the Darcy and the Forchheimer terms, respectively. The symbol K is the porous medium permeability, c_F = 0.55 is the form drag coefficient (Forchheimer coefficient), $\langle \overline{p} \rangle^i$ is the intrinsic average pressure of the fluid and ϕ is the porosity of the porous medium.

The macroscopic Reynolds stress, $-\rho\phi\langle\overline{\mathbf{u}'\mathbf{u}'}\rangle^i$, appearing in Eq. (2) is given as,

$$-\rho\phi\langle\overline{\mathbf{u}'\mathbf{u}'}\rangle^i = \mu_{t_\phi} 2\langle\overline{\mathbf{D}}\rangle^{\mathbf{v}} - \frac{2}{3}\phi\rho\langle k\rangle^i \mathbf{I} \tag{3}$$

where,

$$\langle\overline{\mathbf{D}}\rangle^v = \frac{1}{2}\left[\nabla(\phi\langle\overline{\mathbf{u}}\rangle^i) + [\nabla(\phi\langle\overline{\mathbf{u}}\rangle^i)]^T\right] \tag{4}$$

is the macroscopic deformation tensor, $\langle k\rangle^i = \langle\overline{\mathbf{u}'\cdot\mathbf{u}'}\rangle^i/2$ is the intrinsic turbulent kinetic energy, and μ_{t_ϕ}, is the turbulent viscosity, which is modeled in Pedras and de Lemos (2001) similarly to the case of clear flow, in the form,

$$\mu_{t_\phi} = \rho c_\mu \frac{\langle k\rangle^{i^2}}{\langle\varepsilon\rangle^i} \tag{5}$$

The intrinsic turbulent kinetic energy per unit mass and its dissipation rate are governed by the following equations,

$$\rho\left[\frac{\partial}{\partial t}\left(\phi\langle k\rangle^i\right) + \nabla\cdot\left(\overline{\mathbf{u}}_D\langle k\rangle^i\right)\right] = \nabla\cdot\left[\left(\mu + \frac{\mu_{t_\phi}}{\sigma_k}\right)\nabla\left(\phi\langle k\rangle^i\right)\right] - \rho\langle\overline{\mathbf{u}'\mathbf{u}'}\rangle^i : \nabla\overline{\mathbf{u}}_D + c_k\rho\frac{\phi\langle k\rangle^i|\overline{\mathbf{u}}_D|}{\sqrt{K}} - \rho\phi\langle\varepsilon\rangle^i \tag{6}$$

$$\rho\left[\frac{\partial}{\partial t}\left(\phi\langle\varepsilon\rangle^i\right) + \nabla\cdot\left(\overline{\mathbf{u}}_D\langle\varepsilon\rangle^i\right)\right] = \nabla\cdot\left[\left(\mu + \frac{\mu_{t_\phi}}{\sigma_\varepsilon}\right)\nabla\left(\phi\langle\varepsilon\rangle^i\right)\right] + c_1\left(-\rho\langle\overline{\mathbf{u}'\mathbf{u}'}\rangle^i : \nabla\overline{\mathbf{u}}_D\right)\frac{\langle\varepsilon\rangle^i}{\langle k\rangle^i} + c_2 c_k\rho\frac{\phi\langle\varepsilon\rangle^i|\overline{\mathbf{u}}_D|}{\sqrt{K}} - c_2\rho\phi\frac{\langle\varepsilon\rangle^{i^2}}{\langle k\rangle^i} \tag{7}$$

where, σ_k =1, σ_ε =1.3, c_1 =1.44, c_2 =1.92, c_μ =0.09 and c_k =0.28 are non-dimensional constants defined in Launder and Spalding (1974).

Two Energy Equation Model

The One Energy Equation model is usually valid when the temperature difference between the solid and fluid phase is relatively small. In this case, the condition of Local Thermal Equilibrium (LTE) is applied. When the LTE is far from reality, the one energy equation model needs to be replaced with the two energy equation model, which treats the solid and the fluid phase on separate, via their own macroscopic energy equations Saito and de Lemos (2005). Those equations read:

$$\left(\rho c_p\right)_f\left[\frac{\partial\phi\langle\overline{T_f}\rangle^i}{\partial t} + \nabla\cdot\left\{\phi\left(\langle\overline{\mathbf{u}}\rangle^i\langle\overline{T_f}\rangle^i + \underbrace{\langle{}^i\overline{\mathbf{u}}\,{}^i\overline{T_f}\rangle^i}_{\text{thermal disperson}} + \underbrace{\overline{\langle\mathbf{u}'\rangle^i\langle T_f'\rangle^i}}_{\text{turbulent heat flux}} + \underbrace{\overline{\langle{}^i\mathbf{u}'\,{}^iT_f'\rangle^i}}_{\text{turbulent thermal disperson}}\right)\right\}\right] =$$

$$\underbrace{\nabla\cdot\left[k_f\nabla\left(\phi\langle\overline{T_f}\rangle^i\right) + \frac{1}{\Delta V}\int_{A_i}\mathbf{n}_i\,k_f\,\overline{T_f}\,dA\right]}_{\text{conduction}} + \underbrace{\frac{1}{\Delta V}\int_{A_i}\mathbf{n}_i\cdot k_f\nabla\overline{T_f}\,dA}_{\text{interfacial heat transfer}} \tag{8}$$

where the expansion,

$$\langle\overline{\mathbf{u}'T_f'}\rangle^i = \langle\overline{(\langle\mathbf{u}'\rangle^i + {}^i\mathbf{u}')(\langle T_f'\rangle^i + {}^iT')}\rangle^i = \overline{\langle\mathbf{u}'\rangle^i\langle T_f'\rangle^i} + \langle\overline{{}^i\mathbf{u}'\,{}^iT_f'}\rangle^i \tag{9}$$

has been used in light of the double decomposition concept given by Pedras and de Lemos (2001). For the solid phase, one has,

$$\left(\rho c_p\right)_s \left\{\frac{\partial\left(1-\phi\right)\langle\overline{T_s}\rangle^i}{\partial t}\right\} = \underbrace{\nabla\cdot\left\{k_s\nabla\left[\left(1-\phi\right)\langle\overline{T_s}\rangle^i\right] - \frac{1}{\Delta V}\int_{A_i}\mathbf{n}_i\, k_s\overline{T_s}\, dA\right\}}_{\text{conduction}} \underbrace{-\frac{1}{\Delta V}\int_{A_i}\mathbf{n}_i\cdot k_s\nabla\overline{T_s}\, dA}_{\text{interfacial heat transfer}} \tag{10}$$

where $\langle\overline{T_s}\rangle^i$ and $\langle\overline{T_f}\rangle^i$ denote the intrinsic average temperature of solid and fluid phases, respectively, k_f and k_s are the fluid and solid thermal conductivities, respectively. A_i is the interfacial area within the REV and $\mathbf{n}_i$ is the normal unit vector at the fluid-solid interface, pointing from the fluid towards the solid phase.

Interfacial Heat Transfer

In Eq. (8) and Eq.(10) the heat transferred between the two phases can be modeled by means of a film coefficient h_i such that,

$$h_i a_i\left(\langle\overline{T_s}\rangle^i - \langle\overline{T_f}\rangle^i\right) = \frac{1}{\Delta V}\int_{A_i}\mathbf{n}_i\cdot k_f\nabla\overline{T_f}\, dA = \frac{1}{\Delta V}\int_{A_i}\mathbf{n}_i\cdot k_s\nabla\overline{T_s}\, dA \tag{11}$$

where $a_i = A_i/\nabla V$ is the interfacial area per unit volume. In porous media, the high values of a_i make them attractive for transferring thermal energy via conduction through the solid followed by convection to a fluid stream.

A numerical correlation for the interfacial convective heat transfer coefficient was proposed by Saito and de Lemos, for turbulent flow as:

$$\frac{h_i D}{k_f} = 0.08\left(\frac{Re_D}{\phi}\right)^{0.8} Pr^{1/3};\ \text{for } 1.0x10^4 < \frac{Re_D}{\phi} < 2.0x10^7\ \text{,valid for } 0.2 < \phi < 0.95\,, \tag{12}$$

Using the model shown in Eq. (11) above for the interfacial heat transfer h_i, and Eq.(12), the energy equations (8) and (10) can be rewritten as:

$$\left\{\left(\rho c_p\right)_f \phi\right\}\frac{\partial\langle\overline{T_f}\rangle^i}{\partial t} + \left(\rho c_p\right)_f \nabla\cdot\left(\mathbf{u}_D\langle\overline{T_f}\rangle^i\right) = \nabla\cdot\left\{\mathbf{K}_{eff,f}\cdot\nabla\langle\overline{T}_f\rangle^i\right\} + h_i a_i\left(\langle\overline{T_s}\rangle^i - \langle\overline{T_f}\rangle^i\right) \tag{13}$$

$$\left\{\left(1-\phi\right)\left(\rho c_p\right)_s\right\}\frac{\partial\langle\overline{T_s}\rangle^i}{\partial t} = \nabla\cdot\left\{\mathbf{K}_{eff,s}\cdot\nabla\langle\overline{T_s}\rangle^i\right\} - h_i a_i\left(\langle\overline{T_s}\rangle^i - \langle\overline{T_f}\rangle^i\right) \tag{14}$$

where, $\mathbf{K}_{eff,f}$ and $\mathbf{K}_{eff,s}$ are the effective conductivity tensor for fluid and solid, respectively, given by:

$$\mathbf{K}_{eff,f} = [\phi k_f]\,\mathbf{I} + \mathbf{K}_{disp} \tag{15}$$

$$\mathbf{K}_{eff,s} = [(1-\phi)k_s]\,\mathbf{I} \tag{16}$$

and $\mathbf{I}$ is the unit tensor.

Non-dimensional parameters:

The local Nusselt number for the one-energy equation model as used by Fischer and de Lemos (2008) :

$$Nu = \left(\frac{\partial\langle\overline{T}\rangle^i}{\partial y}\right)_{y=H}\frac{H}{T_1 - T_0} \tag{17}$$

Eq. (17) assumes the local thermal equilibrium hypothesis, i.e., $\langle T\rangle^i = \langle T_s\rangle^i = \langle T_f\rangle^i$. When the Local Non-thermal Equilibrium model is used, that are distinct definitions for the Nusselt number associated to each phase, as follows and are defined as Alazami and Vafai (2000):

Fluid phase Nusselt number:

$$Nu_f = \left(\frac{\partial \langle \overline{T}_f \rangle^i}{\partial y} \right)_{y=H} \frac{H}{T_1 - T_0} \tag{18}$$

Solid phase Nusselt number:

$$Nu_s = \left(\frac{\partial \langle \overline{T}_s \rangle^i}{\partial y} \right)_{y=H} \frac{H}{T_1 - T_0} \tag{19}$$

Depending on the thermal model used, there are two possibilities to evaluate the local wall heat flux q_{wx}. One can use the hypothesis of Local thermal equilibrium (LTE), or else, individual terms can be in each phase applied in order to calculate the integrated heat transferred from the bottom wall, in the latter case, the Local thermal non-equilibrium (LTNE) is employed.

Therefore, for one-energy equation model, one has:

$$q_w = \frac{1}{L}\int_o^L q_{wx}(x)\,dx; \quad q_{wx} = -k_{eff} \left. \frac{\partial \langle T \rangle^i}{\partial y} \right|_{y=H}; \quad k_{eff} = \phi k_f + (1-\phi)k_s \tag{20}$$

For two-energy equation model:

$$q_w = \frac{1}{L}\int_o^L q_{wx}(x)\,dx; \quad q_{wx} = -k_{eff,f} \left. \frac{\partial \langle T_f \rangle^i}{\partial y} \right|_{y=H} - k_{eff,s} \left. \frac{\partial \langle T_s \rangle^i}{\partial y} \right|_{y=H}; \quad \begin{cases} k_{eff,f} = \phi k_f \\ k_{eff,s} = (1-\phi)k_s \end{cases} \tag{21}$$

For the cases where the a porous layer is considered, the wall heat flux is given a superscript ϕ on the form q_w^ϕ. The ratio q_w^ϕ / q_w can be seen as a measure of the effectiveness of using a porous layer for enhancing or damping the amount of heat transferred through the wall.

4. NUMERICAL METHOD

Equations (1), (2), (13) and (14) subject to interface and boundary conditions were discretized in a two-dimensional control volume involving both clear and porous mediums. The equations discretization uses a system of generalized coordinates. The finite volumes method was used in the discretization and the SIMPLE algorithm (Patankar 1980) was used to the treatment of pressure-velocity coupling.

The general and discretized form of the two-dimensional conservation equation of a generic property φ, in permanent regime, is given by:

$$I_e + I_w + I_n + I_s = S_\varphi \tag{22}$$

where I_e, I_w, I_n and I_s represent, respectively, the fluxes of φ in the faces east, west, north and south of the control volume and S_φ its term source.

Every time the source term is dependent of $\langle \varphi \rangle^i$, it will be linearized in the following form:

$$S_\varphi \approx S_\varphi^{**} \langle \varphi \rangle_p^i + S_\varphi^* \tag{23}$$

The source terms in the momentum equations to x direction are given by:

$$S^{*x} = \left(S_e^{*x}\right)_P - \left(S_w^{*x}\right)_P + \left(S_n^{*x}\right)_P - \left(S_s^{*x}\right)_P + S_P^* \tag{24}$$

$$S^{**x} = S_\phi^{**} \tag{25}$$

where, S^{*x} is the diffusive part treated in explicit form. The term S^{**x} in the equation for the porous medium is composed by the term of Darcy coefficient in the x direction.

5. RESULTS AND DISCUSSION

Low Reynolds $k-\varepsilon$ model was used. To ensure the modeling of the flow properties within the laminar sublayer the value of y^+ was kept less than or equal to 1, $(y^+ \leq 1)$. The profile of turbulent kinetic energy (k) at the entrance of the jet was calculated according to the equation:

$$k = \frac{3}{2}(v_0.T_i)^2 \tag{26}$$

where v_0 is the profile of inlet velocity in the channel and T_i is the turbulent intensity. The profile of turbulent kinetic energy dissipation (ε) is obtained by the equation:

$$\varepsilon = c_\mu^{\frac{3}{4}} \frac{k^{\frac{3}{2}}}{l} \tag{27}$$

Where c_μ is the constant of turbulence model described in the mathematical model, k is the kinetic energy of turbulence and l is the turbulence scale.

The fluid properties and the geometric dimensions (figure 2) used for all cases solved in turbulent flow presented are shown in the table below, the diameter used is $D = B$

Table 1 - Parameters used in turbulent flow

Fluid	Especific Mass (ρ)	Viscosity (μ)	B	L	T_0	T_1	Turbulence Scale	Turbulent Intensity
Air	1,225 kg/m^3	1,789x10^{-5} N.s/m^2	14.23 mm	500 mm	309.1 K	347.6 K	0.07B	2%

The influence of the number of nodes of the mesh was checked according to local and global parameters, were calculated the local Nusselt number in the bottom plate and heat flow in the overall lower wall for three mesh configurations, as shown in Table 2, for following parameters $H/B = 2.6$ and Re=10400, since the difference between meshs in relation a mesh of 40×216 nodes (mesh which has a lower number of nodes) this was the mesh used for the turbulent flow. The Figure 3 below illustrates the influence of the mesh in local and global results.

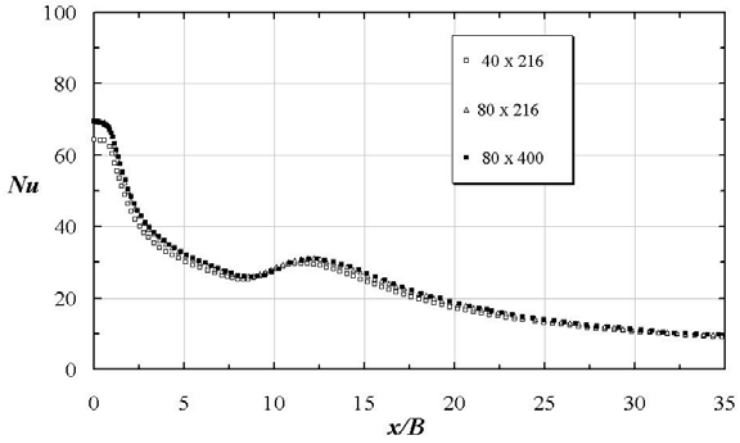

Figure 3 – Validation for distribution of Nu along the lower plate for clear channel effect of grid size

Table 2 – Influence of grid size on integral wall heat flux.

Grid size (nodes)	40x216	80x216	80x400
Wall heat flux q	772.75W	818.87W	825.68W
Deviation in relation to grid 80x400 (%)	6.41%	0.82%	0.0%

All the following results have been simulated with the following geometric configurations and boundary conditions: uniform velocity and temperature profile; inlet jet temperature $T_1 = 309.1K$; the inferior plate temperature is maintained constant and equal to $T_o = 347.6K$; the ratio between the nozzle-to-plate spacing and nozzle width is maintained constant and equal to $H/B = 2.6$; the nozzle width is $B = 1\times10^{-03}m$. The code validation was shown in Dórea and de Lemos (2010b).

The effect of the ratio k_s/k_f is show next. Figure4*a* and Figure 4*b* indicates that k_s/k_f variation does not influence the flow behavior also confirmed by Dórea and de Lemos (2010a) , since a decoupled solution is here applied, or say, the thermal field is solved with constant properties and no buoyancy effects are considered. Corresponding fluid and solid temperature distributions are plotted in Figure5a and Figure5b respectively. For high k_s/k_f cases temperature gradients for both fluid and solid phases decreases since a higher solid thermal conductivity transport heat more easily through the solid, which, in turn, heats up the fluid via interfacial heat transfer. Figure 6 and Figure 7 shows that the higher the ratio k_s/k_f is the lower is the temperature at the wall for both phases, fluid and solid, since is more intense the heat exchange between the phases for high values of k_s/k_f. Figure 8 shows the effect of k_s/k_f and energy model on the local distribution of Nusselt number. It is observed that for low and high k_s/k_f ratios substantially different results with one and two energy equation model are obtained, this result emphasizes the great influence of Reynolds number in the energy model applied, since for low Reynolds number and for low k_s/k_f values temperature profiles of fluid and solid phases are of same order as shown the work of Dórea and de Lemos (2010a). As such, consideration of local thermal equilibrium hypothesis is not realistic for this case.

Figure 9 finally compiles results for q_w^{ϕ}/q_w when the thermal conductivity ratio k_s/k_f and porosity ϕ are varied. It is observed that the one energy equation model overestimates the wall heat flux. Also shown is that for $\phi = 0.9$ the presence of a porous layer is beneficial for k_s/k_f greater than 50, since the ratio q_w^{ϕ}/q_w for such condition is greater than 1 as well as in laminar flow show in Dórea and de lemos (2010a) . However, one should emphasize that differences between the two models, One Energy Equation model and Two Energy Equation model are here obtained under the assumptions mentioned earlier, or say, neglect of tortuosity and local conduction when the LTE and LNTE hypotheses are applied, respectively. These mechanisms might have a certain impact on the final predictions with the two models.

(a)

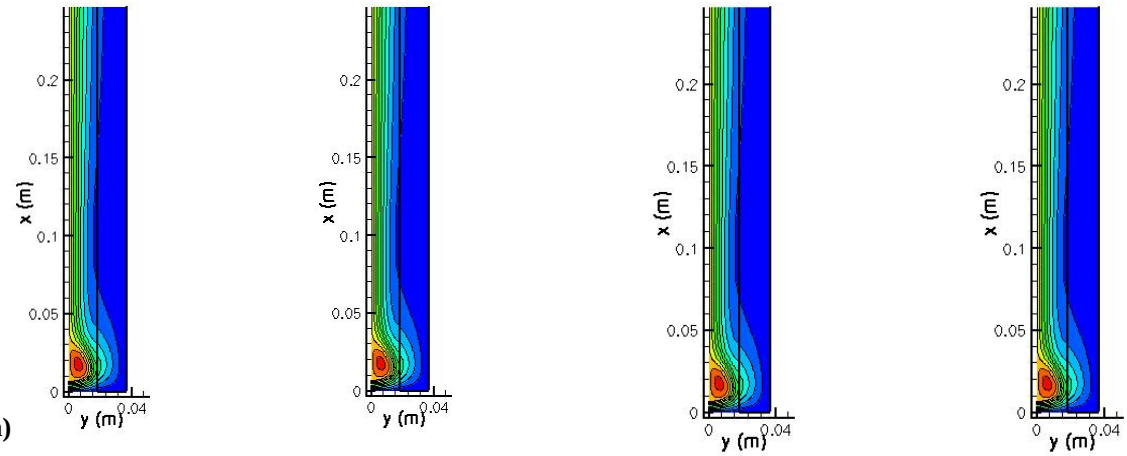

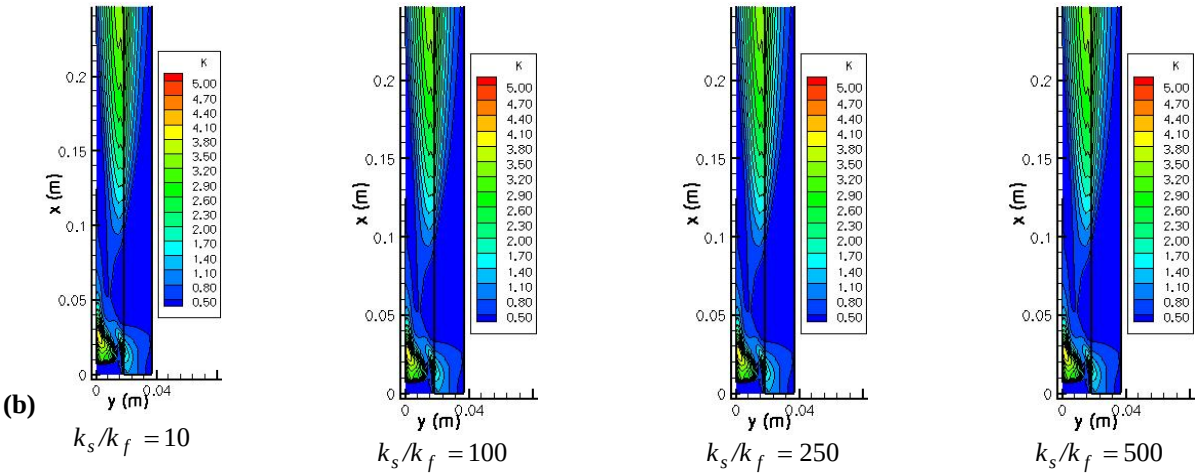

Figure 4 – Flow Behavior maps for various porous thickness layer: (a) Streamlines, (b) Turbulent Kinetic Energy

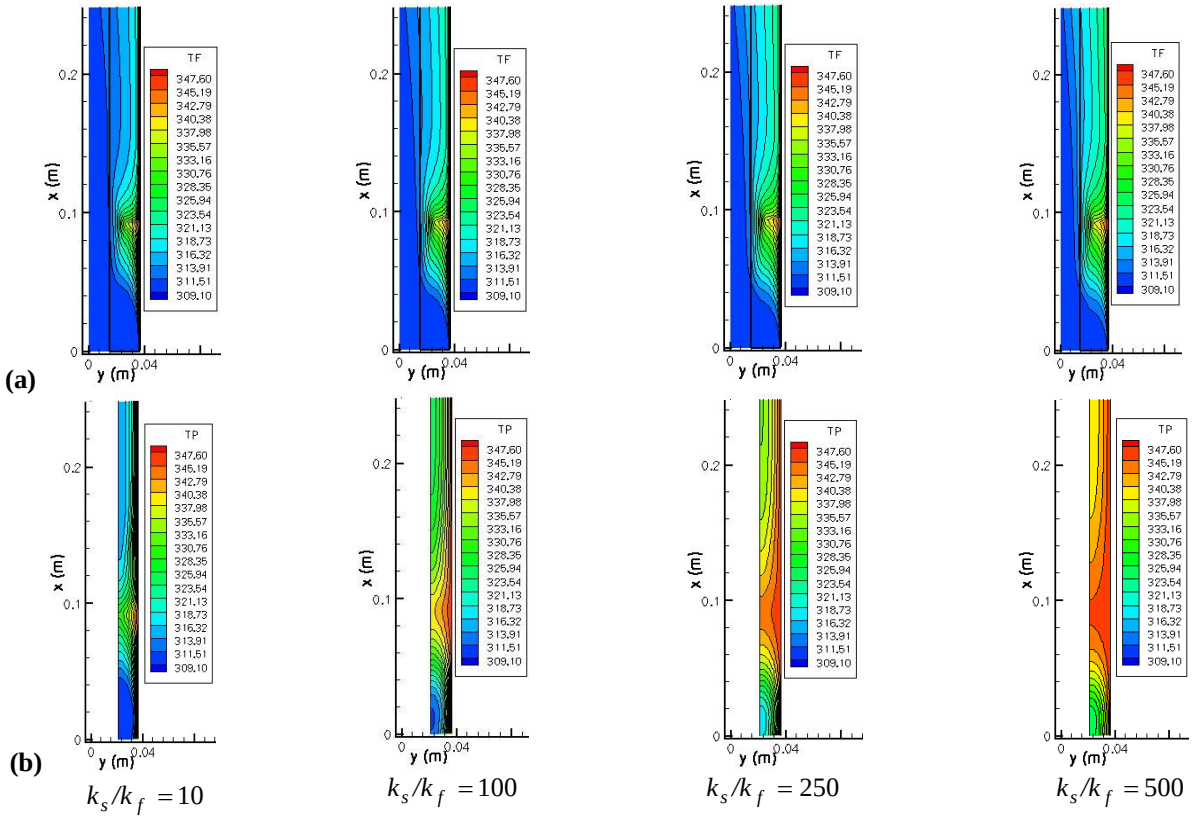

Figure 5 – Thermal Behavior maps for various porous thickness layer: (a) Fluid Temperature, (b) Solid Temperature

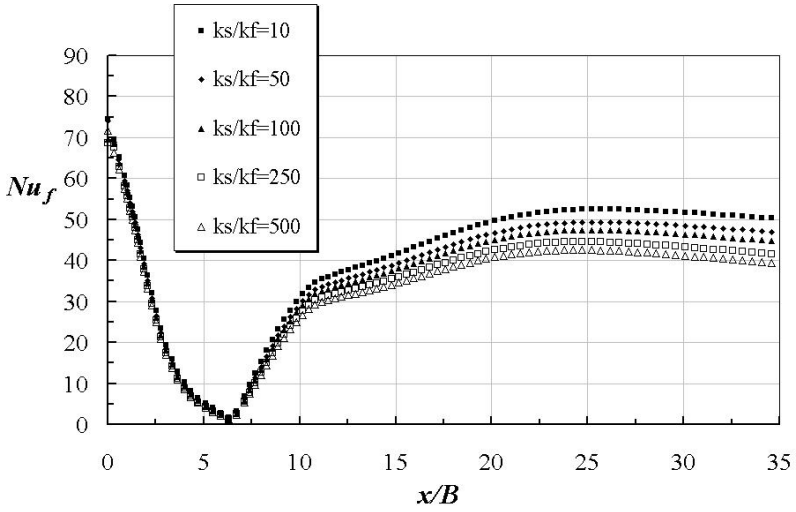

Figure 6 – Distribution of local Nusselt for the fluid phase for various k_s/k_f, with Re=10400, $H/B = 2.6$, $k_s/k_f = 10$, $Da = 8.95x10^{-5}$ and $\phi = 0.9$

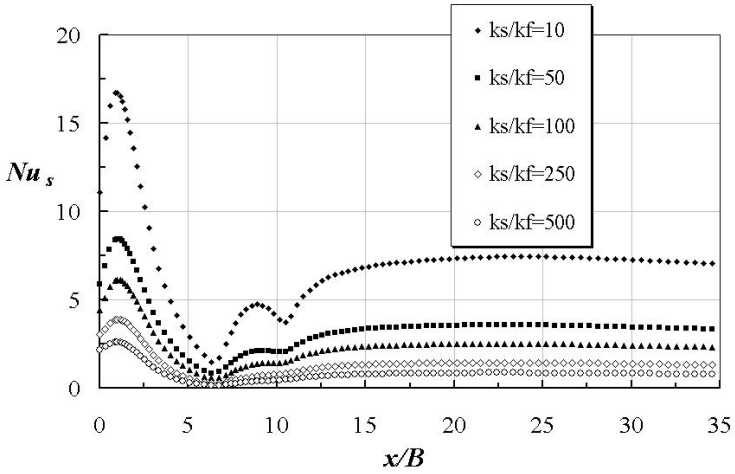

Figure 7 - Solid Nusselt number for various k_s/k_f, with Re=10400, $H/B = 2.6$, $k_s/k_f = 10$, $Da = 8.95x10^{-5}$ and $\phi = 0.9$

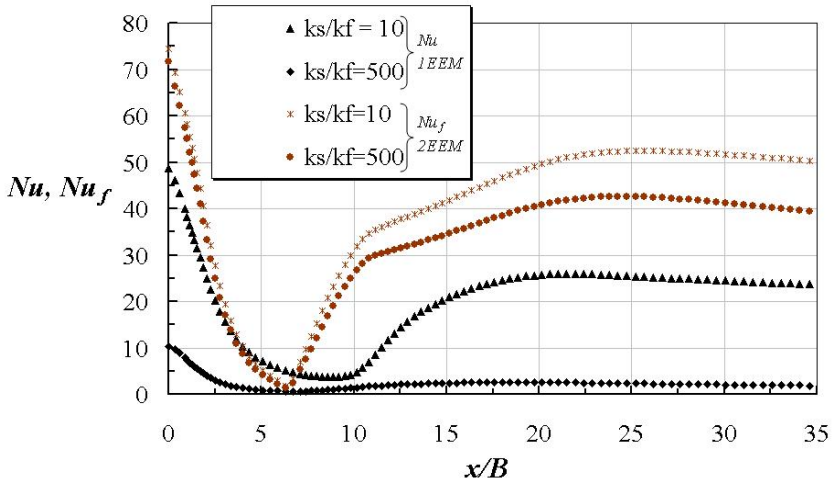

Figure 8 - Distribution of local Nusselt number depending on the model of energy and the ratio of thermal conductivity, $H/B = 2.6$, $\mathrm{Re} = 10400$, $Da = 8.95x10^{-5}$ e $\phi = 0.90$.

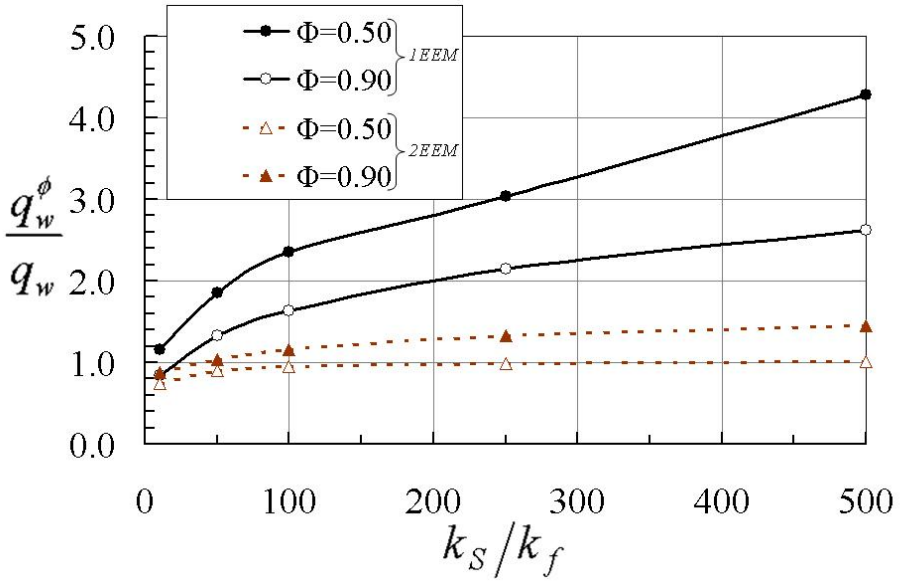

Figure 9 - Integral heat flux at the lower wall for various ratios k_s/k_f in function of energy model applied, for *Re*=10400, $H/B = 2.6$, $Da = 8.95x10^{-5}$, $\phi = 0.5$ and $\phi = 0.9$

6. CONCLUSIONS

This paper investigated the behavior of energy model, one and two energy equations model to simulate heat transfer in a turbulent impinging jet into a porous bed. Effect of solid-to-fluid thermal conductivity ratio were investigated. The following conclusions were observed:

For high k_s/k_f ratios, temperature levels remain high at the solid phase, increasing, consequently, fluid temperatures and, in addition, thickening the thermal boundary layer at the wall.

The use of the LNTE model indicates that it is advantageous to use a layer of highly conducting and highly porous material attached to the cooled wall. However, these conclusions are based under the assumption of neglecting the mechanisms of tortuosity and dispersion within the porous material.

7. ACKNOWLEDGEMENTS

The authors are thankful to CAPES for their financial support during the preparation of this work

8. REFERENCES

Alazmi, Vafai, K. “Analisys of variants within the porous media transport models”. Journal of Heat Transfer, 122 (2000), 303-326.

Assato, M, Pedras, M.H.J., de Lemos, M.J.S., Numerical Solution of Turbulent Channel Flow Past a Backward-Facing-Step with a Porous Insert Using Linear and Non-Linear k-ε Models, Inter. Journal of Heat and Mass Transfer 8 (1) 2005, 13-29.

Chang K.C., Hsieh W.D., Chen C.S., “A modified low-Reynolds-number turbulence model applicable to recirculating flow in pipe expansion”, Transactions of the ASME, Journal of Fluids Engineering 117 (1995) 417-423.

Chen, M., Chalupa, R., West, A.C. and Modi, V., 2000, High Schmidt Mass Transfer in a Laminar Impinging Slot Jet, Inter. J. of Heat and Mass Transfer, Vol.43, pp. 3907-3915.

Chiriac, V.A. and Ortega, A., 2002, Numerical Study of the Unsteady Flow and Heat Transfer in a Transitional Confined Slot Jet Impinging on an Isothermal Surface, Inter. J. of Heat and Mass Transfer , Vol.45, pp. 1237-1248.

Dórea, Felipe Tannús; de Lemos M.J.S.,(2010a)“Escoamento Laminar de jato impingente sobre camada porosa com não-equilíbrio térmico. Parte 2. Efeito da razão de condutividade térmica do sólido pela condutividade térmica do fluido”. In: CONEN2010 - VI Congr. Nacional de Engenharia Mecânica, 2010, Campina Grande, PB, 18-21 Ago. Anais do CONEM2010.

Dórea, Felipe Tannús; de Lemos M.J.S.,(2010b)“Turbulent Impinging Jet Into a Porous bed with thermal non-equilibrium. Part1. Porous Layer Thickness Effect”(Submitted). In: ENCIT2010 - 13th Brazilian Congress of Thermal Sciences and Engineering, Uberlandia, MG, 5-12 Dec. Paper ENC10-0258, ABCM 2010.

Fox, R.W., McDonald, A.T., Introduction to Fluid Mechanics, Wiley, 5th. Ed.1998

Gardon, R. and Akfirat, J.C., 1966, Heat Transfer Characteristics of Impinging Two-Dimensional Air Jets, Journal of Heat Transfer, Vol.101, pp. 101-108.

FrostyTech.com, 2010. 18/05/2010 <FrostyTech.com.>

Graminho, Daniel Rezende ; de Lemos M.J.S., "Simulation of Turbulent Impinging Jet Into a Cylindrical Chamber With and Without a Porous Layer at the Bottom". International Journal of Heat and Mass Transfer, v. 52, p. 680-693, 2009.

Fu, W.-S. and Huang, H.,-C, 1997, "Thermal performance of different shape porous blocks under an impinging jet", International Journal of Heat and Mass Transfer, Vol. 40, No. 10, pp. 2261-2272.

Hsieh W.D., Chang K.C., "Calculation of wall heat transfer in pipe-expansionturbulence flows", International Journal of Heat and Mass Transfer 39 (18) (1996) 3813-3822.

Jeng, T.-Z. and Tzeng, S.-C., 2005, "Numerical Study of Confined Slot Jet Impinging on Porous Metallic Foam Heat Sink", International Journal of Heat and Transfer, Vol.48, pp. 4685-4694.

Kuznetsov, A.V., Cheng, L., Xiong, M., 2002, Effects of thermal dispersion and turbulence in forced convection in a composite parallel-plate channel: Investigation of constant wall heat flux and constant wall temperature cases, Numerical Heat Transfer Part A-Appl., 42(4), 365-383.

Launder, B.E., Sharma B.I., "Application of the energy-dissipation model of turbulence to the calculation of flow near a spinning disc", Letters in Heat and Mass Transfer 1 (1974) 131-138.

Launder, B.E., Spalding D.B., "The numerical computation of turbulent flows", Comp. Meth. Appl. Mech. Eng., 3 (1974) 269-289

Pedras, M.H.J., de Lemos M.J.S. "Macroscopic turbulence modeling for incompressible flow through undeformable porous media". International Journal of Heat and Mass Transfer, New York, v. 44, n. 6, p. 1081-1093, 2001.

Saito; M.B., de Lemos M.J.S., "Interfacial heat transfer coefficient for Non-equilibrium convective transport in porous media." International Communications in Heat and Mass Transfer, New York, v. 32, n. 5, p. 667-677, 2005.

Santos, N.B., de Lemos, M.J.S., 2006. Flow and heat transfer in a parallel-plate channel with porous and solid baffles, Numerical Heat Transfer Part A-Appl., 49(5), 471-494.

Sparrow, E.M. and Wong, T.C., 1975, Impinging Transfer Coefficients due to Initially Laminar Slot Jets, Inter. J. of Heat and Mass Transfer, Vol.18, pp. 597-605.

Wang, S. J. Mujundar, A. S., "A comparative study of five low Reynolds number k-e models for impingement heat transfer", Applied Thermal Engineering 25 (2004) 31-44

Pedras, M.H.J., de Lemos M.J.S. "Macroscopic turbulence modeling for incompressible flow through undeformable porous media". International Journal of Heat and Mass Transfer, New York, v. 44, n. 6, p. 1081-1093, 2001.

Saito; M.B., de Lemos M.J.S., "Interfacial heat transfer coefficient for Non-equilibrium convective transport in porous media." International Communications in Heat and Mass Transfer, New York, v. 32, n. 5, p. 667-677, 2005.

Patankar, S.V., (1980)"Numerical Heat Transfer and Fluid Flow", Hemisphere, New York.

Prakash, M., Turan, F.O., Li, Y., Manhoney, J. and Thorpe, G.R., 2001a, Impinging Round Jet Studies In A Cilindrical Enclosure With And Without A Porous Layer: Part I: Flow Visualizations And Simulations, Chemical Eng. Science, Vol.56, pp. 3855-3878

Prakash, M., Turan, F.O., Li, Y., Manhoney, J. and Thorpe, G.R., 2001b, Impinging Round Jet Studies In A Cilindrical Enclosure With And Without A Porous Layer: Part II: DLV Measurements And Simulations, Chemical Eng. Science, Vol.56, pp. 3879-3892

Van Heiningen A.R.P., "Heat Transfer under an impinging slot jet", Ph.D. Thesis, Department of Chemical Engineering, McGill University, Montreal, Quebec, Canada, 1982.

9. RESPONSIBILITY NOTICE

The authors are the only responsible for the printed material included in this paper.